

1 **MULTI-SCALE ANALYSIS OF THE INFLUENCE OF PHYSICOCHEMICAL**
2 **PARAMETERS ON THE HYDRODYNAMIC AND GAS-LIQUID MASS**
3 **TRANSFER IN GAS/LIQUID/SOLID REACTORS**

4

5

6 A. Kherbeche ^{a,b,c,d,e}, J. Milnes ^{c,d,e}, M. Jimenez ^{c,d,e}, N. Dietrich ^{c,d,e,*}, G. Hébrard ^{c,d,e}, B. Lekhlif ^{a,b}

7

8 ^a Environmental Engineering Laboratory of EHTP , Hassan II University, Morocco

9 ^b Polymer research team, ENSEM, Hassan II University, Morocco

10 ^c Université de Toulouse; INSA,UPS,INP; LISBP, 135 Avenue de Rangueil, F-31077

11 Toulouse, France

12 ^d INRA, UMR792, Ingénierie des Systèmes Biologiques et des Procédés, F-31400

13 Toulouse, France

14 ^e CNRS, UMR5504, F-31400 Toulouse, France

15

16

17

18 * Corresponding Author: Nicolas Dietrich

19 E-mail: Nicolas.Dietrich@insa-toulouse.fr

20

21

22

23

24

25

26 **Abstract**

27 The present paper reports an original, predominantly experimental study of the mass
28 transfer efficiency in biofilters. Hydrodynamic and mass transfer parameters were
29 investigated at two different scales. These parameters have been first considered (i) at a
30 global scale in a three-phase fixed bed reactor with investigating the influence of the
31 physic chemical properties of liquid phase and then (ii) from a local point of view by
32 focusing at the bubble/packing contact. Experiments at global scale have been conducted
33 in a semi-industrial scaled reactor (4.5 m height, 0.15 m in diameter) operating in batch
34 mode, in co-current gas-liquid upflow. Air was injected at the bottom of the reactor
35 through porous disc diffusers. Two kinds of packing, Meteor and Biolite, which have
36 been thoroughly studied by Maldonado et al. (2008), have been tested and compared. The
37 impact of the liquid phase was investigated for different solutions containing clear water
38 and some additives (salts, sugar, suspended solids and varied pH) that can be encountered
39 in industry. For each liquid phase tested, gas holdup, pressure drop, slip velocities and
40 bubble sizes were estimated, as well as volumetric mass transfer coefficients under
41 different superficial gas velocities (ranging from $2.3 \cdot 10^{-3} \text{ m}\cdot\text{s}^{-1}$ to $2.9 \cdot 10^{-2} \text{ m}\cdot\text{s}^{-1}$). For all
42 the tested cases, variations in the hydrodynamic behavior were observed with increasing
43 superficial gas velocity and with all the compounds added to the liquid phase. Mass
44 transfer coefficients decreased with all the tested compounds except for low
45 concentrations of salts, acid and basic solution. Local-scale experiments were performed
46 in a 2D cell made of *PMMA*, with a height of 200 mm, width of 100 mm and thickness
47 of 2 mm, to investigate the visualization of mass transfer and hydrodynamics in the axial
48 profile of bubbles rising through a fixed bed. A high speed camera was used with an
49 oxygen sensitive dye to visualize oxygen transfer and Kalliroscope particles to visualize

50 bubble hydrodynamics. A specific approach was proposed for estimating the mass
51 transfer coefficient in such a configuration. It was found that the mass transfer coefficient
52 k_L depended on bubble behavior through the packing. Low porosity of packing, bubble
53 size and velocity were the principal parameters influencing the hydrodynamics and mass
54 transfer coefficients at this scale.

55 This study considered a new approach to obtain precise data on biofilter systems,
56 investigate the hydrodynamics and gas-liquid mass transfer at two scales, enriching the
57 database on biofilters and providing new insights that could improve this system in
58 industry.

59

60 **Keywords:** Hydrodynamics, Mass transfer coefficient, Complex media, Bubbles,
61 Visualization.

62

63

64

65 **1. Introduction**

66 Usually called biofilters, fixed bed reactors are mainly used for carbon, nitrogen and
67 suspended particle elimination in the aerobic treatment of urban wastewaters. Today they
68 have several applications in industry (Indrani 2005; Chaudhary 2003). In wastewater
69 treatment, biofilters combine compactness and high removal efficiencies. These
70 gas/liquid/solid systems, in presence of pollutants, develop a fixed biomass clinging to
71 the solid phase to purify wastewater. Bacterial activity for wastewater treatment in the
72 biofilter involves several steps (Gullicks et al., 2011), each of which induces a variation
73 in the physicochemical quality of the liquid phase, sometimes limiting performance or, in
74 more critical cases, leading to malfunction.

75 It is well known that the hydrodynamics and gas-liquid mass transfer in bioreactors,
76 where the gas is the dispersed phase, play a key role in the performance of such systems.
77 This performance depends on the amount of oxygen that aeration systems are able to
78 supply to the bacteria that are attached to the fixed packing. Therefore, it is necessary to
79 investigate the effect that variations in the physicochemical quality of the liquid phase
80 during bacterial activity has on the hydrodynamics and mass transfer and to monitor their
81 incidence on the performance of the biofilter.

82 Characterizing hydrodynamics and mass transfer in the presence of biomass or real
83 wastewater is delicate because of the complex nature of such media. As a first approach,
84 it seems thus interesting to consider clear water and suspensions of known constituents
85 that may give a physicochemical quality similar to that of wastewater. Such synthetic
86 media should mainly be composed of salts, organic matter, different kinds of suspended
87 solids and considered at different ranges of pH, and thus viscosities. However even when
88 considering this simplified configuration, difficulties to characterize such systems are

89 many-sided since hydrodynamics and mass transfer are directly linked to numerous
90 parameters such as liquid phase properties, characteristics of the bed, gas injection
91 system, etc. In literature, it has been shown for instance that the gas holdup and pressure
92 drop in packed bubble columns depend on the way the three phases are present in the
93 system. Sundararajan and Ju (1993) explained that hydrodynamics and mass transfer
94 were influenced by three factors:

95 1- Changes of the chemical medium properties by the cells activity,

96 2- Presence of solid particles,

97 3- Mass transfer enhancement by the reaction. Maldonado et al. (2008), Daeosong Ju et
98 al. (2008a, 2011b), and Bhatia et al. (2004) have shown the effect of physical properties
99 of the solid phase. The introduction of a solid phase as a fixed bed in a bubble column
100 affects the size of the bubbles and their behavior. The first parameters that can influence
101 this behavior are the porosity of the packing, the particle diameters and particle density.

102 Many authors have shown that the gas holdup and the volumetric oxygen mass transfer
103 coefficient increase with the superficial air velocity (Maldonado et al.; 2008). The
104 diffuser also has considerable importance for conditioning the hydrodynamics and mass
105 transfer. Hébrard et al. (1996) found that spargers generating small bubbles were the best
106 for promoting mass transfer as their interfacial area was large. Concerning impacts of the
107 liquid composition, several studies focused on diphasic systems. For instance,
108 Jamongwong et al. (2010) treated the effect of salts on a small scale, finding that they
109 affected the size of bubbles and changed their physical interface characteristics, thus
110 modifying the mass transfer by minimizing coalescence phenomena. Studies have also
111 shown the increase of gas holdup when salts are present (Hikita et al., 1974). The

112 addition of organic compounds in the liquid phase is not without effect. Plais et al. (2005)
113 and Dumont et al. (2006) have shown that adding an organic phase dispersed in an
114 aqueous phase decreases the mass transfer. Jamongwong et al. (2010) also tested the
115 effect of glucose in a diphasic system, showing that it decreased the liquid side mass
116 transfer coefficient k_L . The addition of solid micro-particles decreases the volumetric
117 mass transfer coefficient and also the gas holdup in a diphasic system, as was shown by
118 Plais et al. (2005). Omota et al. (2006) studied the effect of the behavior of several types
119 of solid particles (based on carbon and silicate) in gas bubbles. They were shown to affect
120 the way in which the bubble transferred oxygen, in particular that the lower part of the
121 bubble was where oxygen passed to the next stage in the case of with two phases. Lopez-
122 Lopez et al. (2007) found that the pH did not greatly influence the mass transfer or the
123 hydrodynamics, and the viscosity of the liquid phase increased gas holdup and decreased
124 the volumetric mass transfer coefficient by reducing the diffusion coefficient of oxygen
125 in the liquid (Stemmet et al., 2008).

126

127 However, such studies are scarce when considering threephasic systems. The purpose of
128 this paper is thus to compare these conclusions to those obtained in a semi-industrial
129 scaled reactor. Impacts of packing, liquid composition and gas superficial velocity on
130 hydrodynamics and mass transfer have been obtained, analyzed and presented in this
131 paper.

132 But it can be note that when considering this global approach, the behavior between
133 bubbles and packing, which is of prime interest when dealing with mass transfer
134 efficiencies, is delicate to quantify. A second set of experiments have thus been
135 conducted to locally and directly visualize hydrodynamics and mass transfer behaviors in

136 the wake of single air bubbles rising in presence of packing in a simplified 2D Hele-Shaw
137 cell. In the literature, some researchers investigated colorimetric techniques by means of
138 an oxygen or dioxygen carbon sensitive dyes but this approach is very delicate and
139 difficult. In this paper, Two original and promising techniques, colorimetric (for mass
140 transfer) and Kallirosopic (for hydrodynamics) techniques, are developed in this paper
141 to achieve such interesting visualizations in such type of reactors. Based on these
142 visualizations, a comparison in terms of mass transfer efficiency has been performed for
143 two kinds of packing and for different packing orders.

144 By considering global and local experiments, a new and original approach is proposed to
145 go beyond the understanding of the different mechanisms operating in gas/liquid/solid
146 systems.

147

148 .

149

150

151 2. Materials and Methods

152 As mentioned in the introduction, experiments to study the hydrodynamics and mass
153 transfer were carried out on two scales. An almost industrial scale with large dimensions
154 was used to observe the phenomena of hydrodynamics and mass transfer generally and,
155 in parallel, local scale experiments, with dimensions similar to those of the particles of
156 the packing, were performed to search for more precise explanations of the results found
157 at the global scale.

158

159 2.1 Global Scale

160 At the global scale, the experiments were carried out in a fixed-bed column 4.5 m high
161 and 0.15 m in diameter made of transparent PVC. Water and gas were introduced at the
162 bottom of the column. Whatever the operating conditions, the water regime was
163 discontinuous (batch mode) (Figure 1). Two kinds of packing, Meteor and Biolite, were
164 tested and filled the column to a height of 3.5 m. Their physical properties, presented in
165 Table 1, have been studied by Garcia Maldonado (2007).

166 The packing was fixed using a grid. It has been observed that pressure drop caused by the
167 grid was negligible. The liquid phase flow was steady and its physicochemical quality
168 was varied, the concentrations of compounds being chosen among values encountered in
169 the wastewater treatment industry. In the experiments, clear water was used with the
170 addition of some compounds. Thus, the influence of sodium chloride was examined for a
171 range of 1 to 10 g.L⁻¹, then the concentration of glucose was varied from 0 to 50 g.L⁻¹.
172 The influence of suspended matter was investigated using the effect of two products, a
173 clay (bentonite) for concentrations of 0.1 to 1 g.L⁻¹, and suspended carbonaceous

174 material (Acticarbon or powdered coal) at 0.1 to 1 g.L⁻¹. The effect of pH was studied
 175 using sodium hydroxide, NaOH, for basic pH and sulfuric acid, H₂SO₄, for acid pH.
 176 Compressed air was used to inject gas into the column with a porous sparger. The
 177 bubbles leaving the diffuser were between 2 and 6 mm in diameter (Hébrard et al.; 1996)
 178 the superficial velocity of air was varying from 2.3 10⁻³ to 2.9 10⁻² m.s⁻¹ in the column.
 179 The behavior of bubbles inside the column and through the packing were observed with a
 180 high speed camera (Photron SA3), located in the middle of the column at a height of 2.2
 181 m. Images were taken at 500 frames per second. The window is 50mm×50mm.

182 The liquid phase was introduced using a peristaltic pump, filling slowly to drive out any
 183 air bubbles that might have become trapped between packing particles. In all the
 184 experiments, the initial liquid height was kept constant at 3.8 m. Next, the air was
 185 injected. The gas holdup is the volume of gas in the column compared to the total volume
 186 after injection of the gas (Eq.1). In other words, the gas holdup is the difference of water
 187 level observed in the liquid phase before and after gas injection. The volume of gas
 188 retained in the liquid segment is equal to the volume of water displaced and can be
 189 calculated by the following formula (Eq.2):

$$\varepsilon_G = \frac{V_G}{V_T} \quad (1)$$

190

$$\varepsilon_G = \frac{(D_c^2)(h - h_0) + (h_{surv})(D_{surv}^2 - D_c^2) - 4(U_G)(D_c^2)(h - h_0)}{(D_c^2)(H_B)} \quad (2)$$

191

192 For the pressure drop determination, pressure taps were installed along the height of the
193 column, at 0.2m, 2m and 3.5 m from the bottom, and were connected to a U tube.

194 Once the column had been filled with the liquid phase, the oxygen was almost completely
195 stripped from the water by injection of pure nitrogen at very high flow rate through the
196 distributor. A calibrated Mettler-Toledo sensor placed at the top of the column at 3.8 m
197 height showed a value of 0 mg.L⁻¹ at the beginning of the experiments (Figure 1). Air was
198 then sparged into the column and the oxygen was taken up by the liquid phase. The total
199 measurement time was chosen long enough for the oxygen saturation concentration C^* to
200 be reached (about 15 min, a measurement each 5 seconds), the rising curve following the
201 relation (Eq.3):

$$\ln \frac{C^* - C}{C^* - C_0} = -k_L a \cdot t \quad (3)$$

202 The interfacial area depends on the bubble size and is given by Equation 4: (According to
203 the study of Garcia Maldonado et al. (2008), ε_s was given for each packing used)

$$a = \frac{6}{d_b} \cdot \frac{\varepsilon_G}{1 - \varepsilon_G - \varepsilon_s} \quad (4)$$

204

205 Based on high-speed camera acquisitions, bubble diameters, d_b , were easily determined
206 using Equation (5).

$$d_b = (h_b l_b^2)^{1/3} \quad (5)$$

(6)

$$d_{bm} = \frac{\sum_m (d_b^3)}{\sum_m (d_b^2)}$$

207 The average number of bubbles measured was about 200 per configuration. The behavior
208 of bubbles was analyzed and the number of occasions when bubbles coalesced or broke
209 up was calculated in each configuration.

210 The liquid side volumetric mass transfer coefficient k_L was calculated by means of the
211 volumetric mass transfer coefficient k_{La} found in the experiments and the interfacial area.

212 2.2 Local scale

213 Several 2D-packed configurations (called packed channel) were created to represent the
214 3D fixed bed in order to visualize how the bubble hydrodynamics could impact the mass
215 transfer and what the influence of the nature/shape of the packing was. These systems
216 were adapted in a Hele-Shaw cell (0.1×0.1 m visualization chamber made of transparent
217 PMMA (PolyMethylMethAcrylate) with a very small depth of 0.002 m) and the particles
218 were packed vertically to produce a vertical channel for the bubble injected at an orifice
219 at the bottom of the cell (see Figure 2). The size of the bubble was chosen to be around
220 2.5 mm in order to represent the bubble size in biofilters. Four different distances D
221 between particles lines were tested with Meteor (2, 5, 8 and 10 mm) and three with
222 Biolite (2, 4, and 6 mm). A high speed camera was placed in front of the cell, with a
223 shutter speed of 1/1000 s, an acquisition rate of 2000 frames/second.

224 The purpose of this local approach is to observe the hydrodynamics and mass transfer
225 behaviors in the wake of rising bubbles in the configuration presented above just by using
226 a high-speed camera. Two visualization techniques have thus been tested: a colorimetric

227 one for visualizing mass transfer and another with Kalliroscope particles for the
228 hydrodynamics.

229

230 2.3 Kalliroscope technique

231 The local hydrodynamics, which also affects bubble behavior in the packing, was studied
232 by means of a virtual rheoscopic fluid (VRF) called Kalliroscope (Matisse and Gorman,
233 1984). This product is a liquid additive (Andereck et al., 1986) which contains
234 microscopic reflective flakes that orient themselves with bubble flow in 2D cells. The
235 flakes are strongly reflective in some areas and nearly transparent in others which allow a
236 direct visualization of the hydrodynamics behavior in the bubble path. For these
237 experiments a solution with 50% w/w of Kalliroscope in demineralized water has been
238 considered. An example of visualization performed using these particles is presented in
239 Figure 11-a. It can be note that this technique has been used just to visualize the
240 hydrodynamics behavior in the bubble path in order to compare it with mass transfer. No
241 quantification purposes have been considered.

242 2.3 Colorimetric technique

243 The colorimetric technique is based on the use of an oxygen-sensitive dye. Its main
244 advantage is that it is non-intrusive, as the measurements are carried out without
245 disturbing the flow or inserting a physical sensor. There are a large number of organic
246 chemical compounds that present the following properties when subjected to an
247 oxidation/reduction reaction:

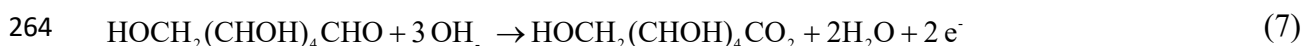
- 248 - intense color in the oxidized or reduced state
- 249 - no color or a different color in the conjugate (opposite) state.

250 For example, methylene blue is blue in the oxidized state but colorless in the reduced
251 state. The well-known “blue bottle” experiments use this property (Cook et al., 1994;
252 Walter et al, 1997; Engerer and Cook, 1999; Wellman and Noble, 2003).

253

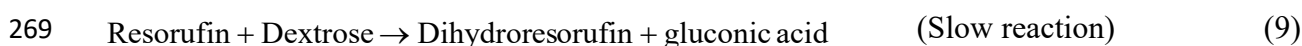
254 In this study, several dyes were tested: methylene blue, indigo carmine and resazurin.
255 Resazurin was finally chosen because it gave a good compromise between speed of the
256 kinetics and color to be achieved. In addition, resazurin is well known as its reduction has
257 been used for about 50 years to monitor bacterial and yeast contamination of milk, and
258 also for assessing semen quality (O’Brien et al, 2000).

259 As shown in Figure 3, resazurin (blue and not fluorescent) is reduced into resorufin (pink
260 and highly fluorescent), which is itself reduced to dihydroresorufin (colorless and not
261 fluorescent). These reactions are catalyzed by the presence of glucose and sodium
262 hydroxide. In alkaline solutions, glucose is oxidized to D-gluconic acid or alpha-D-
263 gluconolactone:



265 $\quad\quad\quad$ (*Dextrose*) $\quad\quad\quad$ (*Gluconic Acid*)

266 The change of color results from the reversible oxidation-reduction reactions between
267 resorufin (pink) and dihydroresorufin (colorless):



270 Note that the complete chemical formula of resazurin is 7-Hydroxy-3H-phenoxazin-3-
271 one-10-oxide (molecular mass 229.19 g.mol⁻¹).

272

273 A preliminary study (not detailed here) was carried out to define the best composition of
274 the catalyst (glucose and sodium hydroxide) in the dye solution, i.e. the one leading to:

- 275 - (quasi)-instantaneous kinetics for the oxidation of dihydroresorufin (colorless)
276 into resorufin (pink),
- 277 - sufficiently slow kinetics (few minutes) for the reduction of resorufin (pink)
278 into dihydroresorufin (colorless),
- 279 - high colorimetric yield (i.e. the color intensity).

280

281 From this, the following formulation was chosen: glucose and sodium hydroxide were
282 both diluted at 20 g.L^{-1} in deionized water, and the concentration of resazurin was fixed
283 at 0.1 g.L^{-1} .

284 Based on this technique and just by using a high-speed camera, the mass transferred in
285 the bubble wake could easily be visualized since a darker area appeared on the recorded
286 image (darker area representing the pink form of the dye and thus the presence in
287 oxygen). An example of such a visualization is proposed in Figure 4-a.

288

289 2.4 Image processing

290 Based on this kind of images (Figure 4-a), a specific approach has been developed to
291 quantify this mass transferred in the bubble wake to compare efficiencies for the different
292 tested configurations. To achieve this quantification, the first step was to establish a
293 calibration curve between the “grey level” observed on the recorded image and the
294 corresponding oxygen concentration. For this, several colorimetric solutions were
295 prepared at different concentrations of resazurin (0.05 and 0.01 g.L^{-1}). They were

296 saturated in oxygen with air in order to reach their highest intensity of pink (or their
297 highest value of grey level on the acquired image). For each colorimetric solution flowing
298 in the cell (without bubbles), about 50 pictures were recorded and averaged. In addition,
299 images were acquired when no oxygen was present in the colorimetric solution. The third
300 averaged images obtained showed how the grey level changed according to the resazurin
301 concentration (Figure (5-b)).

302 The stoichiometry of the reaction between oxygen and dihydroresorufin is given by
303 Equation 8. Then, the number of moles of dissolved oxygen can easily be deduced from
304 the number of moles of resazurin, as

$$305 \quad n_{O_2,transferred} = n_{O_2,reacted} = \frac{n_{dihydroresorufin}}{2} = \frac{n_{resazurin}}{2} \quad (10)$$

306 Thus, for each resazurin concentration (0, 0.05 and 0.1 g.L⁻¹), it was possible to associate
307 the observed averaged grey level with a dissolved oxygen concentration. The calibration
308 curve obtained is plotted in Figure 5-a. The perfect linearity observed between grey level
309 and dissolved oxygen concentration is remarkable and is an undeniable advantage of this
310 method. It is also important to note that this calibration curve is attached to the present
311 experimental set-up and conditions. In other words, if a change was made in the light or
312 camera parameters, the calibration would have to be performed again. Based on this
313 calibration curve, grey levels recorded by the camera could thus be converted into oxygen
314 concentration. However further efforts have to be considered before achieving accurate
315 quantification. A specific image processing, whose only the basic principles are presented
316 in this paper, has thus been developed. An example of raw image to be corrected is
317 depicted in Figure 4-a. As a first step, an image reference is subtracted to the raw image.
318 This reference image is an image without any bubble or mass transfer. By subtracting
319 these two images, packing and impurities on the picture have been removed (see Figure

320 4-b). However due to some temporal non-homogeneities of the lighting, the background
321 grey level (and oxygen concentration) could differ from 0. The background grey level
322 had thus to be set to 0 to not alter mass transfer calculations. On the resulting image (See
323 Figure 4-c), only remain the bubble and its mass transferred. Bubble edges have been
324 detected using specific algorithms (Canny edge detector, extracted from Image
325 Processing Toolbox in Matlab®). Bubbles edges have thus been detected (Figure 4-d)
326 and removed (Figure 4-e) from the corresponding image. Figure 4-e represents an
327 example of corrected image where non null pixels represented a certain amount of
328 oxygen transferred by the bubble. The total amount of mass transferred could easily be
329 determined by considering the estimated concentration pixel per pixel.

330

331 **3. Results at global scale**

332 The results of the gas holdup experiments are reported as a function of gas velocity in
333 Fig. 7. It is clear that, whatever the type of solid, the gas holdup increases with increasing
334 superficial gas velocity U_G , for all the liquid phases tested. Gas holdup was also found to
335 depend on physical characteristics of the packing, such as the apparent porosity, particle
336 size (as was shown by Garcia Maldonado (2007)). For a packing of low porosity, breakup
337 occurs and no large bubbles form, (Moustiri et al.; 2002). Thus the contact area between
338 particles and bubbles is large (Maldonado et al.; 2008). The reduction induced in the slip
339 velocity therefore increases the gas holdup. This is shown in Figure 7-b, where gas hold-
340 up values reported for Biolite range between 0.04 and 0.07, while the values for Meteor
341 are between 0.01 and 0.05, the range of superficial gas velocity U_G being from 0.0023
342 m.s^{-1} to 0.0117 m.s^{-1} in both cases.

343 Concerning the influence of the physicochemical properties of the liquid phase, as shown
344 in Figures 7-a, 7-b and 7-c, it is clear that, for Meteor, the addition of salts (from 1 to 10
345 g.L⁻¹) increases the gas holdup from 0.017 to 0.064 for the same gas flow rates ($U_G =$
346 0.0023 m.s^{-1}) and from 0.067 to 0.128 for high gas flow rates ($U_G = 0.029 \text{ m.s}^{-1}$). Salt
347 addition acts on the bubble behavior by causing an increase in the surface tension and
348 viscosity of the liquid (Jamongwong et al.; 2010). Then, numerous small static bubbles
349 were observed to be embedded between packing particles (see section 2) due to the high
350 surface tension, which reduced the coalescence, especially for high concentrations of
351 salts. It was also noted that the way gas holdup increased with salt concentration
352 depended on the type of packing for the same gas superficial velocity. In fact, figure 7-c
353 shows that the rate of increase of gas holdup for Biolite was lower than that observed in
354 Meteor.

355 The addition of glucose did not have any great effect on gas hold-up. In Fig7-c, it is clear
356 that gas holdup tends to stabilize at high concentrations of glucose (10 to 50 g.L⁻¹): with
357 $U_G = 0.0023 \text{ m/s}$, it does not exceed 0.026 for the Meteor and 0.048 for the Biolite.
358 Adding glucose decreased the surface tension of the liquid and this was the principle
359 cause of a small decrease in the gas hold up even for higher concentrations with the same
360 superficial gas velocity.

361 The suspended solid micro particles added to the liquid phase increased the gas holdup
362 smoothly, as illustrated in figures 7-a and 7-b. Increasing the concentration of bentonite
363 from 0.3 to 1 g.L⁻¹ decreased gas holdup from 0.023 to 0.017. Explanations have been
364 given for the micro scale by Omota et al. (2006), who used coal powder with the liquid
365 and gas. They considered the contact area of the small particles used but did not give
366 results concerning the direct effect of the presence of these particles on gas holdup. The

367 effect of coal powder (Acticarbon) on gas holdup was the same in the present work. Gas
368 holdup varied from 0.02 to 0.014 for concentrations ranging from 0.3 to 1 g.L⁻¹. Finally,
369 the pH did not have a marked effect on gas holdup; the difference of values with pure
370 water did not exceed 0.3% but gas holdup with an acidic liquid phase was slightly less
371 than for the basic liquid phase.

372 The pressure drop measured at the top of the column in our experiments increased due to
373 the increase in gas superficial velocities. Pressure drops for Meteor varied from 0.8 % to
374 8 % when superficial velocity varied from 0.0023 to 0.029 m.s⁻¹ whereas, for Biolite, it
375 ranged between 1 % and 10 %. Bed porosity, contact area and particle shape factor were
376 the parameters that most influenced pressure drop. Increasing doses of salts and glucose
377 increased the pressure drop by about 1 % and 5 % relative to clean water. The suspended
378 solid micro particles increased the pressure drop by about 4 % for bentonite and 0.5 % for
379 Acticarbon.

380 Due to increasing gas holdup, the slip velocity decreased with increasing gas superficial
381 velocity.

$$G = \frac{U_G}{\varepsilon_G} \quad (11)$$

382 Generally, slip velocities in experiments carried out on Biolite were lower than on Meteor
383 (Table 3) because the low porosity bed led to high gas holdup and low slip velocities. The
384 bubbles could be assumed to be broken by interaction with the wire of the packing and
385 the large density of small, uniform-sized bubbles was maintained. The higher values of
386 gas holdup and the uniform bubble size can explain the decrease in slip velocity in the
387 presence of packing. With high doses of salts (10 g.L⁻¹) and thus increased surface

388 tension, small bubbles became more rigid and led to high values of gas holdup. This
389 explains the decrease of almost 10% in slip velocity in the presence of salts. However, for
390 glucose (50 g.L⁻¹), slip velocity decreased due the increase in the viscosity of the liquid
391 by almost 8 % in Meteor. Suspended solids did not strongly influence slip velocity
392 because of the low concentrations of bentonite and coal powder used in the experiments.

393 Experiments showed that the interfacial area calculated from equation (4) increased with
394 the superficial gas velocity (Fig. 8-a) for all liquid phases under test. The interfacial area
395 results are shown as a function of gas velocity in Fig. 8. The interfacial area depends on
396 the bubble diameter and it has also been shown that the influence of the solid phase is
397 critical to bubble diameter and behavior. In fact, within the Meteor bed it was observed
398 that the bubbles in the column were composed of three populations (Fig.6-a). The first
399 kind of bubble encountered was small bubbles, not exceeding 2 mm, clinging to the static
400 packing. Even at high superficial gas velocity, these bubbles became static, mainly when
401 the surface tension of liquid phase was strong, as with highest concentrations of salts.
402 Small bubbles were rigid and fixed in the packing. These kinds of bubbles, also
403 influenced by the porosity of the packing and the particle shapes, were at the origin of the
404 gas holdup results. The second population of bubbles had sizes between 2 and 6 mm,
405 which were generally dynamic. Variations in the liquid characteristics influenced this
406 population. The third population was composed of large bubbles (air pockets) of sizes
407 greater than 6 mm, which were always moving through the bed, sometimes taking small
408 bubbles with them. Their average behavior was usually determined by the bed porosity
409 and the physicochemical quality of the liquid phase, and also by the superficial gas
410 velocity.

411 Compared to Meteor, the bubbles observed in Biolite (Fig.6-b) were always the same.
412 Bubbles were seen to be constantly in movement, mainly because of the very low
413 porosity of Biolite. The contact time between bubbles and packing was long, thus
414 encouraging coalescence among bubbles moving in the packing. It was found that
415 interfacial area on Meteor was higher than that found on Biolite (Fig 8-b).

416 Concerning the superficial gas velocity effect, it was found that increasing superficial gas
417 velocities increased interfacial area, a result also reported by Maldonado (2007), Bhatia
418 (2004) and Moustiri (2002) (Fig. 8-a, 8-b).

419 The study of the effect of the physicochemistry of the liquid phase revealed that, in
420 different salt concentrations (from 1 to 10 g.L⁻¹) for the case of Meteor, it was difficult to
421 see the calculated difference in bubble sizes. The average did not change, so it was hard
422 to say that bubble size changed with concentration of salts. On the other hand, it is
423 possible that the salinity influenced bubble surface characteristics indirectly by changing
424 the coalescence rate between bubbles. A low concentration of salts would make bubble
425 surfaces more favorable to coalescence, while high concentrations of salts would lead to
426 small, more rigid bubbles and increase the attachment of these bubbles to the particles of
427 packing, thus giving the biggest gas holdup in the experiments. The number of small,
428 static bubbles for a concentration of 1 g.L⁻¹ of salt was 8% whereas for 10 g.L⁻¹, their
429 number rose to 35%, which explains the reduction of coalescence phenomena as the
430 interfacial area was then largest (Fig 8-c). Concerning added glucose, it must have
431 changed the liquid viscosity, mainly for high concentrations (from 10 to 50 g.L⁻¹). In this
432 interval, bubble sizes in Meteor were found to be slightly smaller, and the average varied
433 from 3.32 to 2.32 mm with a superficial gas velocity $U_G = 0.0023 \text{ m.s}^{-1}$. Glucose acted
434 indirectly on the surface of bubbles by reducing the liquid viscosity. Bubbles were then

435 smaller and the interfacial area larger. Suspended solids have a key effect on the surface
436 of bubbles, which depends on the nature of the suspended solids added. In our case, for
437 bentonite, the processed images showed that bubble sizes changed, decreasing from 2.63
438 mm to 2.35 mm for Meteor. For coal, the bubble sizes decreased from 2.19 mm to 1.93
439 mm, but this was not observed for Biolite. It is important to mention that Omota et al.,
440 (2006) found that coal powder could be spread around the bubble and limit the transfer,
441 mainly in the zone beneath the bubble. The pH did not have any great influence on
442 bubble size.

443 The results concerning the volumetric mass transfer coefficient $k_L a$ in Figure 9 show that
444 increasing superficial gas velocity increases $k_L a$. The same result has been found in many
445 works concerning tri-phasic systems (Maldonado (2007), Bhatia (2004) and Moustiri
446 (2002)). The effect of the solid phase is crucial in mass transfer. Values of $k_L a$ with
447 Biolite were slightly higher than for the Meteor in this work (Fig.9.b). The gas holdup,
448 which influences the interfacial area, gave values of $k_L a$ between 0.0013 and 0.0151 s^{-1}
449 for Biolite. These values were always higher than those for Meteor, which gave values
450 between 0.0013 and 0.0128 s^{-1} in the range of superficial gas velocity between 0.0023
451 and 0.0029 $m.s^{-1}$. The hydraulic regime was strongly influenced by the nature of the
452 solid. There was little difference between $k_L a$ for low flows whereas, for high flow rates,
453 differences could reach 0.002 s^{-1} .

454 The physicochemical quality of the liquid phase influenced the mass transfer coefficient
455 obtained for a constant gas flow ($U_G = 0.0023 m.s^{-1}$). Up to 10 $g.L^{-1}$ for Meteor (Fig.9-c),
456 the salt addition increased the mass transfer to 0.0028 s^{-1} and, with a maximum of 5 $g.L^{-1}$
457 for Biolite, it also reached 0.0028 s^{-1} . For higher salt concentrations (10 to 50 $g.L^{-1}$), the
458 mass transfer coefficient decreased dramatically. The trends observed previously for the

459 behavior of bubbles confirm the findings for mass transfer evolution: the phenomena of
460 coalescence and breakup were present and the transfer was greater when superficial gas
461 velocities were large. As noted previously, salts acted on the surface of bubbles. At low
462 concentrations (less than 10 g.L⁻¹), oxygen transfer was higher because the bubble
463 surfaces became more active, and that explains the higher k_{La} found. High concentrations
464 of salt induced an increase in the liquid surface tension, allowing smaller and more rigid
465 bubbles to become embedded among packing particles.

466 The effect of glucose on the mass transfer was negative. For low concentrations of
467 glucose, the mass transfer coefficient increased to 0.0026 s⁻¹ for Meteor and 0.0025 s⁻¹ for
468 Biolite. Then, beyond a certain concentration, mass transfer was observed to drop until it
469 reached 0.0016 s⁻¹. It has been seen that the interfacial area was larger and coalescence
470 and breakup were lower for both packed beds. Adding glucose enhanced the viscosity of
471 the liquid phase, thus allowing a decrease in slip velocity that could explain these values
472 of k_{La} . Jamongwong et al. (2010) studied the effect of glucose on the liquid side mass
473 transfer coefficient and found that glucose decreased k_{La} in the small scale gas/liquid
474 system. Asgharpour et al. (2010), and Bhatia et al. (2004) found that the effect of organic
475 solvents and contaminants influenced the mass transfer coefficient negatively. Results
476 were the same for both gas/liquid and gas/liquid/solid column reactors.

477 k_{La} was negatively influenced by the presence of suspended solids. Bentonite decreased
478 k_{La} from 0.0022 s⁻¹ for a null bentonite concentration $C_B = 0$ g.L⁻¹ to 0.0019 s⁻¹ for $C_B =$
479 1g.L⁻¹, while coal had a dramatic effect on transfer values up to 0.0013 s⁻¹ at $C_B = 1$ g.L⁻¹.
480 Omota (2006) observed the negative effect of suspended solids on the adhesion of solid
481 micro-particles to the gas. In our case, the packing acted as a block for suspended solids
482 and this could promote streaking of coal micro-particles on the surface of bubbles. This

483 may have limited the phenomena at the interface of the bubble and may have decreased
484 the gas / liquid mass transfer. It was also shown that the coal (Acticarbon) decreased the
485 transfer more than bentonite did (Fig.9-a). The effect of pH did not influence the transfer
486 greatly: it was found that with a pH of 9.79, there was a slight decrease in $k_{L,a}$, 1%
487 compared to that of water (pH = 7.56), while at pH 3.5, there was an increase of 1% in
488 $k_{L,a}$.

489 It was found that the liquid side mass transfer coefficient increased when slip velocities
490 were higher and allowing higher slip velocity could increase k_L . This result confirms
491 Maldonado et al.'s findings calculated values of k_L encountered for Biolite were slightly
492 higher than those found in Meteor (Table 3). It was also found that, for lower
493 concentrations of salt and glucose, k_L increased by 80 % for both types of packing for the
494 same superficial gas velocity ($U_G = 0.0023 \text{ m.s}^{-1}$) and it decreased by about 60% for high
495 concentrations. Bentonite and Acticarbon both increased the k_L by about 40 % but, for
496 higher concentrations, it was found that k_L decreased. This was due to the interfacial area
497 calculated with the real bubble size encountered in each experiment.

498 **4. Results at local scale**

499 First experiments conducted for this local approach were based on the hydrodynamics
500 behavior in the bubble wake for different spaces D between particles (Figure 2) using
501 Kalliroscope particles. It was observed that, without packing particles, bubbles (2.5 mm
502 diameter, velocity of 0.188 m/s.) followed a zigzag path, leaving a Karman vortex street
503 in their wake (Fig 10.a). Adding particles laterally to the bubble injection did not affect
504 the hydrodynamic structure until a distance between particles of about 10 mm was
505 reached, where the trajectories were clearly impacted as shown in figure 10-b. It was

506 observed that a distance greater than three times the bubble diameter was not interesting
507 for visualizing an impact of the packing.

508 It has been observed that in presence of Meteor particles, the bubble tended to oscillate
509 strongly between particles (Fig 11-a) in comparison with the absence of packing (Fig 10-
510 a). These perturbations in the wake of the bubbles were also visible in the colorimetric
511 technique raw images (Fig 11-b). The observations on the mass transferred by the bubble
512 confirm the experiment on hydrodynamics using the Kallirosopic particles mentioned
513 above. Oscillating rising was also observed and this movement was also present in the
514 bubble wake; the oxygen concentration field followed the streamline. Image processing
515 using Matlab® software calculated the total amount of oxygen dissolved in the wake of
516 the bubble as:

$$517 \quad \bar{m} = \iiint C(x, y) \cdot dx \cdot dy \cdot dz \quad (12)$$

518 These values and the bubble properties (size, velocity) are reported in table 4. As
519 observed in figure 11-b, more than ten times as much oxygen was transferred for the 2-
520 mm channel (3.85×10^{-8} mg) as the 10-mm channel (1.65×10^{-9} mg). This difference could
521 be explained by the smaller bubble velocity in the 2-mm channel and by the impact of the
522 packing geometry, which increased the agitation in the wake, renewing the bubble
523 surface. In contrast, Biolite particles are nearly circular, and this caused a disturbance but
524 not with the same intensity as for Meteor (Fig 11-a). The amount of oxygen was also
525 smaller, ranging from 2.54×10^{-8} mg for the 2-mm channel to 8.03×10^{-9} for the 6-mm
526 channel (Table 4).

527 The shape of the packing bed played a key role. More oxygen was transferred with
528 Meteor than with Biolite for the same channel diameter. This may have been due to the

529 velocity of the bubbles, observed to be higher in Biolite than in Meteor, changing the
530 contact time of the bubble in the cell. The kallirosopic technique, by providing the
531 hydrodynamic structure, confirmed that the wake structure for Meteor led to a better
532 mixing in the channel, improving the efficiency of the transfer. These experiments
533 showed the important contribution made by the packing in a biofilter; the filter particles
534 characterized the movement and behavior of bubbles within the biofilter, which
535 influenced the mass transfer inside the system.

536 The purpose of this final section is to evaluate the liquid-side mass transfer coefficient
537 (k_L) from the dissolved oxygen concentration fields presented above (Fig 5.).

538 As established by Roudet et al. (2011), the volumetric mass flux of oxygen from gas to
539 liquid along a channel can be expressed as:

$$540 \quad \varphi(X') = u_B \cdot \frac{\partial \bar{C}}{\partial X'} \quad (13)$$

541 where X' is the axial position in the channel such that $X' = 0$ at the location where the
542 bubbles are generated and $X' = 0.2$ m at the exit of the channel. \bar{C} is the average
543 concentration in dissolved oxygen accumulated in the channel (mainly in the bubble
544 wake) at the axial position X' along the vertical channel. Assuming that the concentration
545 of dissolved oxygen in the liquid at the scale of the unit cell is zero due to its
546 consumption by the chemical reaction, the mass flux of oxygen (per unit of liquid
547 volume) can also be expressed by:

$$548 \quad \varphi(X') = k_L \cdot a \cdot C^* \quad (14)$$

549 where k_L is the liquid-side mass transfer coefficient, a the interfacial area between gas
 550 and liquid phases and C^* the dissolved oxygen saturation concentration ($C \sim 8 \text{ mgL}^{-1}$).

551 By coupling Equations 13 and 14, relationship 15 is found:

$$552 \quad \frac{\partial \bar{C}}{\partial X'} = \frac{k_L \cdot a \cdot C^*}{u_B} \quad (15)$$

553 If the oxygen transferred at the bubble formation is neglected, integrating Equation 15
 554 over the entire cell gives:

$$555 \quad \bar{C} = \frac{k_L \cdot a \cdot X' \cdot C^*}{u_B} \quad (16)$$

556 In order to estimate the interfacial area, a , between the gas and liquid phases, a
 557 cylindrical shape is assumed for a bubble between the two walls. This is true only for
 558 bubbles having diameters bigger than the thickness of the cell (i.e. 2 mm in our case).

559 With these assumptions, the specific interfacial area for the liquid film a is given by:

$$560 \quad a = \frac{\pi \cdot d_B \cdot e}{V_{channel}} = \frac{\pi \cdot d_B}{X' \cdot D} \quad (17)$$

561 The order of magnitude of the interfacial area, a , goes from 50 to 500 $\text{m}^2 \cdot \text{m}^{-3}$. As
 562 expected (Yue et al, 2007), the values of a are significantly higher than in usual gas–
 563 liquid macro-contactors such as our global scale experiments. They are almost the same
 564 as in static mixers and smaller than in microchannels.

565 The oxygen transferred by a single bubble can then be tracked by the dissolved oxygen
 566 accumulation in the cell, as:

$$567 \quad \bar{C} = \frac{\bar{m}}{V_{channel}} = \frac{\iiint C(x, y).dx \cdot dy \cdot dz}{X.D.e} \quad (18)$$

568 Equation 18 does not take the dimension z , related to the channel width, into account for
 569 integrating C . This is because the present colorimetric technique is not able to
 570 discriminate the visualizations at different planes along the channel width. Consequently,
 571 we should keep in mind that the oxygen concentration fields visualized are the result of
 572 all the different fields existing at all the vertical locations.

573 Finally, from Equations 16 and 17, the liquid-side mass transfer coefficient can be
 574 calculated as:

$$575 \quad k_L = \frac{\bar{C} \times u_B}{X' \times a \times C^*} \quad (19)$$

576 The variation of k_L with gas flow rate is plotted in figure 13 (the associated numerical
 577 values being reported in Table 4). A decrease in the mass transfer coefficient is observed
 578 with an increase in particle distance. This decrease is attributable to the decrease in the
 579 slip bubble velocity.

580

581 In order to validate the colorimetric technique, the liquid-side mass transfer coefficients
 582 above should be compared to those found in the literature and especially with the liquid-
 583 side mass transfer coefficients from Higbie's penetration theory as:

$$584 \quad k_L = 2 \sqrt{\frac{D}{\pi \cdot t_C}} \quad (20)$$

585 Rather good agreement with Higbie's model is observed ($\sim 3 \times 10^{-5}$ m/s), demonstrating
586 how this new visualization technique (easy to implement as without a laser source) can
587 bring new insights for investigating mass transfer processes in a packed bed. Although
588 some experimental aspects remain to be perfected, these original results provide new
589 insight into a theoretical model and numerical simulation.

590

591 4. Conclusion

592 The effect of the physicochemical composition of the liquid phase on hydrodynamics and
593 gas-liquid mass transfer was studied on two scales: a bubble packed-bed column on
594 global scale and a Hele Shaw cell on a local scale. On the global scale, clean water was
595 used with addition of some compounds like salts, sugar, pH modifying compounds, and
596 suspended solids. Several measurement techniques were employed to obtain a good
597 characterization of the hydrodynamic parameters and mass transfer characteristics under
598 various operating conditions. Two kinds of packing were used. Superficial gas velocity
599 was varied in the range of $2.3 \cdot 10^{-3} \text{ m.s}^{-1}$ to $2.9 \cdot 10^{-3} \text{ m.s}^{-1}$. It was found that the
600 physicochemical properties of the liquid phase, the superficial gas velocity and the
601 physical characteristics of the solid phase all had an effect on hydrodynamics and mass
602 transfer.

- 603 - The increase in superficial gas velocity increased gas holdup and mass transfer
604 coefficient. An increase was also observed in the interfacial area, which was
605 independent of the quality of liquid or solid phase in the biofilter.
- 606 - High concentrations of salts increased gas holdup, decreased bubble size and thus
607 increased interfacial area. The mass transfer coefficient increased up to a
608 concentration of 10 g.L^{-1} and then decreased dramatically.
- 609 - Glucose had a slight impact on gas holdup. It was shown that, with high
610 concentrations of glucose, gas holdup increased a little.. Both superficial area and
611 mass transfer decreased with glucose.

612 - Two kinds of suspended solids were used, bentonite and Acticarbon. They
613 increased gas holdup but decreased the mass transfer coefficient. Acticarbon was
614 shown to have more effect on mass transfer than bentonite.

615 - pH did not have a big impact on hydrodynamics. Gas hold up and interfacial area
616 were shown to stay stable for acidic and basic pH. It was found that mass transfer
617 increased with pH.

618 To gain insight into this extraordinary complexity involving hydrodynamics, mass
619 transfer, and interfacial phenomena, some preliminary results were obtained within a 2D-
620 device by means of a newly developed technique. These new experimental results
621 prefigure some possibilities to develop and validate modeling and simulations. At this
622 scale, it has been shown that the oxygen transferred depends on the porosity of the
623 packing, and the arrangement of packing particles. It also depends on the bubble-packing
624 contact time. The present study has clearly highlighted the need to complete the database
625 related to oxygen diffusion coefficients in biofilters. It can give more information about
626 how to improve water and wastewater treatment efficiencies.

627 This study thus constitutes a striking example showing that this new colorimetric method
628 could be an interesting tool for investigating gas-liquid mass transfer in transparent
629 fluids, with a view to reactor design. This information gives new insight into the complex
630 mechanism of bubble mass transfer and could help to develop rigorous theoretical models
631 and numerical simulations.

632

633

634

635 **Acknowledgement**

636 This study was supported by the United Nations Educational, Scientific and Cultural
637 Organization – UNESCO for young researchers in the Water Science Domain.

638

639 **Nomenclature**

a	<i>Interfacial area (m^{-1})</i>
C	<i>Dissolved oxygen concentration at time t ($g.l^{-1}$)</i>
C^*	<i>Dissolved oxygen saturation concentration ($g.l^{-1}$)</i>
C_i	<i>Concentration of compounds ($g.l^{-1}$)</i>
D	<i>Distance between two particles lines in the Hele-Shaw cell = channel size (m)</i>
d_b	<i>Single Bubble diameter (mm)</i>
d_{bm}	<i>Mean bubble diameter (mm)</i>
D_c	<i>Column diameter (m)</i>
D_{surv}	<i>Overflow column diameter (m)</i>
e	<i>Hele-Shaw cell thickness (m)</i>
G	<i>Slip velocity ($m.s^{-1}$)</i>
h	<i>Height of water after gas injection (m)</i>
h_0	<i>Height of water before gas injection (m)</i>
H_B	<i>Bed height (H_B) (m)</i>
h_b	<i>Height of bubble (mm)</i>
H_L	<i>Liquid height (m)</i>
h_{surv}	<i>Height of water on overflow (m)</i>
H_T	<i>Total height (m)</i>
k_L	<i>Liquid-side mass transfer coefficient ($m.s^{-1}$)</i>
$k_{L,a}$	<i>Volumetric mass transfer coefficient (s^{-1})</i>
l_b	<i>Width of bubble (mm)</i>
$PMMA$	<i>PolyMethylMethAcrylate</i>

<i>PVC</i>	<i>Polyvinyl chloride</i>
u_B	<i>Bubble rising velocity ($m.s^{-1}$)</i>
U_G	<i>Gas superficial velocity ($m.s^{-1}$)</i>
V_G	<i>Gas volume (m^3)</i>
<i>VRF</i>	<i>virtual rheoscopic fluid</i>
V_T	<i>Total volume (m^3)</i>
ε_G	<i>Gas holdup</i>
ε_S	<i>Solid hold up</i>

640

641

642 **Table legends**

Table 1.	Physical packing characteristics (Garcia Maldonado, 2007)
Table 2.	Effect of superficial gas velocity on the volumetric mass transfer coefficient k_{La} for both types of packing
Table 3.	Evolution of hydrodynamics and mass transfer for different liquid phases ($U_G = 0.0023 \text{ m/s}$)
Table 4.	Bubble properties at local scale

643

644 **Figure legends**

Figure 1	Global scale experimental setup.
Figure 2	Local scale experimental setup
Figure 3	Principle of the colorimetric technique
Figure 5	Calibration procedure (a) Calibration curve between gray level and dissolved oxygen concentration (b) Variation of the gray level in the Hele-shaw cell for different resazurin concentrations
Figure 4	Image processing. (a) raw image (b) corrected image after subtraction of the background (c) corrected image after subtraction of the noise contribution (d) detection of the bubble contour (e) dissolved oxygen concentration field obtained after applying the calibration curve
Figure 6	Packing used at global scale (a) Meteor (b) Biolite P.3.5
Figure 7	Evolution of gas holdup (a) Gas holdup with all the compounds at 1g.l^{-1} for Meteor versus superficial gas velocity for Meteor (b) Comparison between gas hold up for clean water, NaCl (1g.l^{-1}), glucose (1g.l^{-1}), Acticarbon (1g.l^{-1}) in Meteor and Biolite (c) Evolution of gas holdup with concentration (g.l^{-1}) at superficial gas velocity of 0.0023 m.s^{-1}
Figure 8	Evolution of interfacial area (a) with all the compounds at 1g.l^{-1} for Meteor versus superficial gas velocity for Meteor , (b) Comparison between interfacial area for clean water, NaCl (1g.L^{-1}), glucose (1g.L^{-1}), Acticarbon (1g.L^{-1}) in Meteor and Biolite (c) Evolution of interfacial area with

	concentration (g.L^{-1}) at superficial gas velocity of 0.0023ms^{-1}
Figure 9	Evolution of volumetric mass transfer coefficient k_{La} (a) with all the compounds at 1g.l^{-1} for Meteor versus superficial gas velocity for Meteor, (b) Comparison between volumetric mass transfer coefficient k_{La} for Clean water, NaCl (1g.L^{-1}), glucose (1g.L^{-1}), Acticarbon (1g.L^{-1}) in Meteor and Biolite (c) Evolution of volumetric mass transfer coefficient k_{La} with concentration (g.L^{-1}) at superficial gas velocity of 0.0023m.s^{-1}
Figure 10	Visualization of bubble rise hydrodynamics by kallirosopic technique (a) without packing (b) with packing
Figure 11	Visualization of hydrodynamics and oxygen transfer of bubble rising in Meteor (a) hydrodynamics visualization by kallirosopic technique for bubble rising in Meteor (b) mass transfer visualization by colorimetric method for bubble rising in Meteor.
Figure 12	Visualization of hydrodynamics and oxygen transfer of bubble rising in Biolite (a) hydrodynamics visualization by Kallirosopic technique for bubble rising in Biolite (b) mass transfer visualization by colorimetric method for bubble rising in Biolite
Figure 13	Mass transfer coefficient evolution with channel size for Meteor and Biolite packings

645

646

647 **References**

- 648 Andereck, C.D., Liu, S. S., Swinney, H. L., 1986. Flow regimes in a circular couette
649 system with independently rotating cylinder, *Fluid Mechanic Journal* 4, 155–183.
- 650 Asgharpour, M., Mehrnia, M-R., Mostoufi, N., 2010. Effect of surface contaminants on
651 oxygen transfer in bubble column reactors, *Biochemical Engineering Journal*, 49, 351-
652 360.
- 653 Bhatia, B., Nigama, K.D.P., Aubanb, D., Hébrard, G., 2004. Effect of a new high porosity
654 packing on hydrodynamics and mass transfer in bubble columns, *Chemical Engineering
655 and Processing* 43 , 1371–1380.
- 656 Chaudhary, D.S., Vigneswaran, S., Ngo, H.H., Shim, W.G., and Moon, H., 2003. Biofilter
657 in Water and Wastewater Treatment, *Korean Journal of Chemical Engineering* 20(6),
658 1054-1065.
- 659 Cook, A. G., Tolliver, R. M., Williams, J. E., 1994. The blue bottle experiment revisited
660 gives some details of the reaction mechanism and alternative dyes. *J. Chem. Educ.* 71,
661 160.. DOI:10.1021/ed071p160
- 662 Daeseong, J., Revankar, S.T., 2011. Investigation of bubble breakup and coalescence in a
663 packed-bed reactor – Part 1:A comparative study of bubble breakup and coalescence
664 models, *International Journal of Multiphase Flow* 37, 995–1002.
- 665 Daeseong, J., Revankar, S.T., 2011. Investigation of bubble breakup and coalescence in a
666 packed-bed reactor – Part 2: Development of a new bubble breakup and coalescence
667 model, *International Journal of Multiphase Flow* 37, 1003–1012.
- 668 Dumont, E., Andrès, Y., Le Cloirec, P., 2006. Effect of organic solvents on oxygen mass
669 transfer in multiphase systems: Application to bioreactors in environmental protection,
670 *Biochemical Engineering Journal* 30, 245–252.

671 Engerer, S.C, Gilbert Cook, A., 1999. The Blue Bottle Reaction as a General Chemistry
672 Experiment on Reaction Mechanisms. *J. Chem. Educ.* 76 (11), 1519. DOI:
673 10.1021/ed076p1519

674 Garcia Maldonado, J.G., Bastoul, D., Baig, S., Roustan, M., Hébrard ,G., 2008. Effect of
675 solid characteristics on hydrodynamic and mass transfer in a fixed bed reactor operating
676 in co-current gas–liquid up flow, *Chemical Engineering and Processing* 47 , 1190–
677 1200.

678 Gullicks, H., Hasibul, H., Das, D., Moretti, C., and Yung-Tse Hung, Y.-T., 2011. Biofilm
679 Fixed Film Systems *Water* 3, 843-868.

680 Hébrard G. Etude de l'influence du distributeur de gaz sur l'hydrodynamique et le
681 transfert de matière gaz liquide des colonnes à bulles ; Thèse d'état , 1996.

682 Hikita, H., Kikukawa, H., 1974. Liquid phase mixing in bubble columns: effect of liquid
683 properties, *Chemical Engineering Journal* 8, 191-197.

684 Indrani, D., Grant Allen, D., 2005. Biofilter technology. *Biotechnology for Odor and Air*
685 *Pollution Control*, 125-146.

686 Jamnongwong, M., Loubiere, K., Dietrich, N., Hébrard, G., 2010. Experimental study of
687 oxygen diffusion coefficients in clean water containing salt, glucose or surfactant:
688 Consequences on the liquid-side mass transfer coefficients, *Chemical Engineering*
689 *Journal* 165, 758–768.

690 Lopez-Lopez, J.-S., Benbelkacem, H., Debellefontaine, H., 2007. Influence of *t*-butanol
691 and of pH on hydrodynamic and mass transfer parameters in an ozonation process,
692 *Chemical Engineering and Processing* 46 649–655.

693 Matisse, P., Gorman, M., 1984. Neutrally buoyant anisotropic particles for flow
694 visualization, *Physics of Fluids*, 27(4):759–760.

695 Moustiri, S., Hebrard, G., Roustan, M., 2002. Effect of a new high porosity packing on
696 hydrodynamics of bubble columns , *Chemical Engineering and Processing* , 41, 419-
697 426.

698 O'Brien J., Wilson, I., Orton, T., Pognan, F., 2000, Investigation of the Alamar Blue
699 (resazurin) fluorescent dye for the assessment of mammalian cell cytotoxicity, *Eur. J.*
700 *Biochem.* 267, 5421-5426

701 Omota, F., Dimian, A.C., Bliiek, A., 2006. Adhesion of solid particles to gas bubbles. Part
702 elling, *Chemical Engineering Science* 61, 823 – 834.

703 Omota, F., Dimian, A.C., Bliiek, A., 2006. Adhesion of solid particles to gas bubbles. Part
704 2: Experimental, *Chemical Engineering Science* 61, 835 – 844.

705 Plais, C., Billet, A.-M., Carine, J.-L., Delmas, H., 2005. Etude du transfert gaz-liquide en
706 présence d'une troisième phase finement divisées, *Récents Progrès en Génie des*
707 *Procédés* 92.

708 Roudet, M., Loubière, K., Gourdon, C., Cabassud, M., 2011, Hydrodynamics and mass
709 transfer in inertial gas-liquid flow regimes through straight and meandering
710 millimetric square channels, *Chem. Eng. Sci.* 66 2974-2990.

711 Stemmet, C.P., Bartelds, F., van der Schaaf, J., Kuster, B.F.M., Schouten, J.C., 2008.
712 Influence of liquid viscosity and surface tension on the gas–liquid mass transfer
713 coefficient for solid foam packings in co-current two-phase flow chemical engineering
714 research and design 86, 1094–1106.

715 Sundararajan, A., Ju, L.-K., 1993. Biological oxygen transfer enhancement in bioreactors,
716 *TransIChemE* 71 , 221–223.

717 Walter R. Vandaveer, I.V., Mel Mosher, 1997. The blue bottle revisited. *J. Chem. Educ.*
718 74 (4), 402.. DOI: 10.1021/ed074p402.

719 Wellman, W. E., Noble, M.A., 2003. Greening the Blue Bottle. *J. Chem. Educ.* 80 (5),
720 537,. DOI: 10.1021/ed080p537.

721 Yue, J., Chen, G., Yuan, Q., Luo, L., Gonthier, Y., 2007. Hydrodynamics and mass
722 transfer characteristics in gas–liquid flow through a rectangular microchannel. *Chem.*
723 *Eng. Sci.* 62, 2096–2108.

724

725

726